Table II. Visible and Near-Ultraviolet Spectra

Assignment[b]	Abs max[c]	Solvent
	$Co(acac)_2N_3NH_3$[a]	
$^1T_{1g} \leftarrow {}^1A_{1g}$	17.2 (2.02)	CH_3OH
$\pi_L^* \leftarrow t_{2g}$	33	CH_3OH
$e_g^* \leftarrow \sigma_L$	38.9 (4.04)	CH_3OH
	$Co(acac)_3$[d]	
$\pi^* \leftarrow \pi$	38.6 (4.48)	C_2H_5OH
$\pi^* \leftarrow \pi$	33.9 (4.0)	C_2H_5OH
$\pi^* \leftarrow {}^1A_{1g}$	30.6 (3.9)	C_2H_5OH
$^1T_{2g} \leftarrow \pi$, $^1T_{2g} \leftarrow {}^1A_{1g}$	25.0 (2.5)	C_2H_5OH
$^1T_{1g} \leftarrow {}^1A_{1g}$	16.9 (2.1)	C_2H_5OH

[a] L. J. Boucher and D. R. Herrington, *Inorg. Chem.*, 11, 1772 (1972). [b] L refers to the pentanedionate ligand. [c] log ϵ_{max} given in parentheses. [d] R. L. Lindvedt in "Concepts of Inorganic Photochemistry", A. W. Adamson and P. D. Fleischauer Ed., Wiley-Interscience, New York, N.Y., 1975.

Their assignments and those for $Co(acac)_3$ may be found in Table II. The 350-nm exciting radiation lies entirely within the broad band at 303 nm which has been assigned to a charge transfer to ligand (CTTL) transition involving the pentanedionate ligand. It seems unlikely, however, that this band is a single electronic transition. The similarity between the positions of the lowest energy spin-allowed ligand field transition of $Co(acac)_3$ ($^1T_{1g} \leftarrow {}^1A_{1g}$) and the equivalent transition in $Co(acac)_2N_3NH_3$ suggests that both the charge transfer to metal (CTTM) transition involving the pentanedionate ligand and the ligand field transition ($^1T_{2g} \leftarrow {}^1A_{1g}$) are also contained under the envelope of this band. In addition, the optical electronegativity of the azido group (2.8)[29] is somewhat greater than that of the pentanedionate ligand (2.7).[30] It is therefore expected that the CTTM transition involving the azido group should occur about 3.0×10^3 cm^{-1} higher energy than the same transition involving the pentanedionate ligand. Thus the CTTM state involving the azido group is also contained under the envelope of the band at 303 nm. It is reasonable to assume that a CTTM state involving the azido group is responsible for the observed photochemical reaction. However, the presence of such a large number of transitions in this region makes any further interpretation unwarranted without further investigation.

Although 350-nm radiation populates a number of ligand field and charge transfer excited states, it appears that only the CTTM state(s) involving the azido group gives rise to photodecomposition. The reaction occurs with relatively low quantum efficiency. However, this cannot be attributed to secondary recombination since this process is insignificant under the conditions used in the determinations. In contrast to other simpler cobalt(III)–azido complexes, the photochemical behavior of $Co(acac)_2N_3NH_3$ is uncomplicated by other photochemical reactions.

Acknowledgment. Acknowledgment is made to the donors of the Petroleum Research Fund, administered by the American Chemical Society, and to the National Aeronautics and Space Administration for the support of this research.

Registry No. *cis*-$Co(acac)_2N_3NH_3$, 38977-23-0; $Co(acac)_2$, 14024-48-7.

References and Notes

(1) G. J. Ferraudi and J. F. Endicott, *J. Am. Chem. Soc.*, **95**, 2371 (1973).
(2) J. F. Endicott, M. Z. Hoffman, and L. S. Beres, *J. Phys. Chem.*, **74**, 1021 (1970).
(3) W. Beck and K. Schorpp, *Angew. Chem., Int. Ed. Engl.*, **9**, 753 (1970).
(4) C. Bartocci and F. Scandola, *Chem. Commun.*, 531 (1970).
(5) G. J. Ferraudi and J. F. Endicott, *Inorg. Chem.*, **12**, 2389 (1973).
(6) J. L. Reed, F. Wang, and F. Basolo, *J. Am. Chem. Soc.*, **94**, 1773 (1972).
(7) H. D. Gafney, J. L. Reed, and F. Basolo, *J. Am. Chem. Soc.*, **95**, 7998 (1973).
(8) J. L. Reed, H. D. Gafney, and F. Basolo, *J. Am. Chem. Soc.*, **96**, 1363 (1974).
(9) J. I. Zink, *Inorg. Chem.*, **14**, 446 (1975).
(10) N. Filipescu and H. Way, *Inorg. Chem.*, **8**, 1763 (1969).
(11) D. W. Barnum, *J. Inorg. Nucl. Chem.*, **21**, 221 (1961).
(12) D. W. Barnum, *J. Inorg. Nucl. Chem.*, **21**, 183 (1962).
(13) R. L. Lintvelt in "Concepts of Inorganic Photochemistry", A. W. Adamson and P. D. Fleischauer, Ed., Wiley-Interscience, New York, N.Y., 1975, pp 316–321.
(14) I. Burak and A. Treinin, *J. Chem. Phys.*, **39**, 189 (1963).
(15) W. D. Closson and H. B. Gray, *J. Am. Chem. Soc.*, **95**, 237 (1973).
(16) H. H. Schmidtke, *J. Chem. Phys.*, **45**, 305 (1965).
(17) T. J. Boucher and D. R. Herrington, *Inorg. Chem.*, **11**, 1772 (1972).
(18) J. B. Ellan and R. O. Ragsdale, *Inorg. Synth.*, **11**, 82 (1960).
(19) M. Tinland and H. Flygare, *Z. Anorg. Chem.*, **262**, 328 (1950).
(20) D. Katakis and A. O. Allen, *J. Chem. Phys.*, **38**, 1359 (1964).
(21) D. Watt and J. D. Chrisp, *Anal. Chem.*, **24**, 2006 (1952).
(22) $Rh(NH_3)_5NH_2Cl^{3+}$ generated by the photolysis of $Rh(NH_3)_5N_3^{2+}$ in HCl does not appear to react with $(C_2H_5)_2NH_2BF_4$.
(23) T. S. Roche and J. F. Endicott, *Inorg. Chem.*, **13**, 1575 (1974).
(24) T. S. Roche and J. F. Endicott, *J. Am. Chem. Soc.*, **94**, 8622 (1972).
(25) $\Phi_{Co(II)} = k_4/(k_4 + k_3)$.
(26) A. Treinin and E. Hayon, *J. Chem. Phys.*, **50**, 538 (1969).
(27) T. T. Kelly and J. F. Endicott, *J. Am. Chem. Soc.*, **94**, 1797 (1972).
(28) H. H. Schmidtke and D. Garthoff, *J. Am. Chem. Soc.*, **89**, 1317 (1967).
(29) C. K. Jorgenson, *Acta Chem. Scand.*, **16**, 2406 (1962).

Contribution from the Department of Chemistry, Massachusetts Institute of Technology, Cambridge, Massachusetts 02139

Spectroscopic Studies of the Photoactive $^4T_{2g}$ Excited State of Hexaamminechromium(III)

RANDALL B. WILSON and EDWARD I. SOLOMON*

Received October 14, 1977

Detailed low-temperature, high-resolution polarized single-crystal spectroscopic studies on the $^4T_{2g} \leftarrow {}^4A_{2g}$ transition for a new class of $Cr(NH_3)_6^{3+}$ molecular crystals are described. The $^4T_{2g}$ excited state is experimentally shown to undergo both large totally symmetric and Jahn–Teller distortions. These produce the approximate change in the geometry of the $^4T_{2g}$ excited state relative to the $^4A_{2g}$ ground state of an expansion of 0.12 Å in Cr–NH_3 bond lengths along two axes and a contraction of 0.02 Å along the third axis. The photochemical implications of these distortions are discussed.

I. Introduction

Octahedral chromium(III) complexes form the most well-characterized inorganic systems in terms of their photochemistry.[1] The photochemical studies to date strongly support the $^4T_{2g}$ state as being primarily responsible for the observed photoactivity. The photosubstitution reaction pathways often differ from those of the ground state, and an extensive amount of data has led to empirical rules[2] and ligand

0020-1669/78/1317-1729$01.00/0

field models[3,4] which predict the stereochemistry of the photoreaction. Considering the important stereochemical role associated with the $^4T_{2g}$ excited state in the photolabilization of chromium complexes, it would seem that the experimental determination of the $^4T_{2g}$ excited-state geometry relative to that of $^4A_{2g}$ ground state for a photochemically active chromium complex is now in order.

This study reports detailed high-resolution, low-temperature polarized single-crystal spectroscopic studies on the $^4T_{2g} \leftarrow {}^4A_{2g}$ transition in $Cr(NH_3)_6^{3+}$. In general, broad-band absorptions of inorganic complexes do not show much structure even at liquid-helium temperatures. In order to perform the detailed spectroscopy necessary for this study, a new class of transition-metal hexaammine molecular crystals had to be prepared and characterized.[5] This is summarized in the next section. After a description of our experimental system in section III, the spectroscopic results and theory involved will be presented in parallel in section IV. Our approach in this section will emphasize the determination of all necessary parameters *experimentally*, eliminating our need to rely on any specific model. We will find that both reasonably large Jahn–Teller and totally symmetric distortions occur in the $^4T_{2g}$ state, relative to the ground state. The photochemical implications of these results are discussed in section V.

II. $Cr(NH_3)_6(ClO_4)_2Cl{\cdot}KCl$ Molecular Crystal

A detailed spectroscopic analysis of the photoactive $^4T_{2g}$ state of $Cr(NH_3)_6^{3+}$ requires electronic and vibronic fine structure to be discernible on the broad-band transition to this state. It has been our experience[6] that frequently the amount of structure observed on a band at low temperature is very dependent upon the particular crystal lattice. For this reason, many different salts of $Cr(NH_3)_6^{3+}$ were investigated in order to find those which would be most appropriate for a high-resolution spectroscopic study. From these investigations we found one salt which was unique in showing a very structured $^4T_{2g} \leftarrow {}^4A_{2g}$ transition. In addition, the crystal series to which this salt belongs has the advantage of allowing a variable low-symmetry perturbation at the metal site by variation of counterions in the lattice.

This previously unreported salt, $Cr(NH_3)_6(ClO_4)_2Cl{\cdot}KCl$, is uniaxial, belongs to space group $R\bar{3}m$, and has a D_{3d} site symmetry at the chromium ion.[5] This salt is one in the isomorphic series $M(NH_3)_6(ClO_4)_2X{\cdot}M'X$ ($M = Cr^{3+}, Co^{3+}, Rh^{3+}$; $X = Cl^-, Br^-$; $M' = K^+, Rb^+, Cs^+, NH_4^+$). The crystal structure determination[5] of the $Co(NH_3)_6(ClO_4)_2Cl{\cdot}KCl$ salt shows that the lattice contains linear arrays of $-K-Cl-O_3ClO-(NH_3)_3Cr(NH_3)_3-OClO_3-Cl-$. EPR and absorption measurements to be discussed indicate that upon changing M′, the low-symmetry D_{3d} distortion of the $Cr(NH_3)_6^{3+}$ ion decreases in the order $K^+ > Rb^+ > Cs^+$. The "amount" of structure observed on the $^4T_{2g} \leftarrow {}^4A_{2g}$ transition upon changing X and M′ follows the order $Cl^- > Br^-$ and $K^+ \sim Rb^+ > Cs^+ \sim NH_4^+$.

Large single crystals of $Cr(NH_3)_6(ClO_4)_2Cl{\cdot}KCl$ were grown by slow evaporation (in the dark) of solutions prepared by dissolving stoichiometric amounts of twice recrystallized $Cr(NH_3)_6Cl_3$, $Cr(NH_3)_6(ClO_4)_3$, and KCl in 0.03 M HCl. The crystals form hexagonal plates with the face normal to the crystallographic *c* axis.

III. Experimental Section

Our optical system is a McPherson RS-10 1-m double-beam recording spectrometer which has been extensively modified to allow polarized, low-temperature spectra to be obtained on very small crystals. This system utilizes interchangeable sources, gratings, and detectors in combination with a PMT feedback loop and log ratiometer to effectively cover the region 2.5–0.2 μm. The standard curved chopping mirror is replaced with a custom-designed planar mirror, and lenses are used to focus the beam through a matched set of Glan-Taylor polarizers onto the sample and then refocus the beam onto the detector. Focusing at the detector becomes important in the near-IR, where a PbS detector with minimal surface area is used to maximize the S/N ratio. An interchangeable lens system was optimized with respect to lens materials and focal lengths for a given region, and only one interchange of lenses is required to cover the entire spectral range. Problems with Wood's anomalies and a wavelength-dependent baseline were overcome by careful alignment of all optical components and balancing of the two beams.

Low temperatures from 2 to 300 K are obtained using a Janis Research Super Vari-Temp liquid-helium Dewar with Suprasil W optical windows. A Lakeshore Cryogenics (Model DTC-500) temperature controller and silicon diode (DT-500P) are used for temperature regulation, and a calibrated silicon diode mounted near the sample allows measurement of the sample temperature to better than 1 K. An X–Y translation mounting of the Dewar combined with a removable detector housing on the spectrometer allows easy visual alignment of the sample, which can be as small as 1 mm × 0.3 mm.

IV. $^4T_{2g} \leftarrow {}^4A_{2g}$ Transition

A. Electronic Spectroscopy. The σ, π, and α single-crystal polarized absorption spectra of the $^4T_{2g} \leftarrow {}^4A_{2g}$ transition of $Cr(NH_3)_6(ClO_4)_2Cl{\cdot}KCl$ at 6 K are shown in Figure 1. Comparison of the three polarizations demonstrates that the broad transition is electric dipole allowed ($\sigma = \alpha \neq \pi$) and shows one dominant progression with a spacing of about 403 cm^{-1}. The intensity decreases with decreasing temperature, indicating it is vibronically allowed, as is expected for a molecule with a center of inversion. The band starts with a group of weak, magnetic dipole allowed ($\pi = \alpha \neq \sigma$) origins centered around 5011 Å; these are split into two groups separated by about 15 cm^{-1} as shown in Figure 1c. The corresponding lines in the RbCl salt also have a splitting of about 15 cm^{-1} but are somewhat broader and less polarized (Figure 2). The bands immediately higher in energy from the magnetic dipole lines are electric dipole allowed and shift in energy on going from the KCl (Figure 1c) to the RbCl salt (Figure 2). No other magnetic dipole allowed transitions to either higher or lower energy (within 1000 cm^{-1}) were observed.

We assign the magnetic dipole lines as the pure electronic origins of the $^4T_{2g}$ state. In part B, we determine the splitting of these electronic origins which would be expected (based on experimental parameters) in the absence of Jahn–Teller effects.

B. Electronic Splitting of the $^4T_{2g}$ Origins. The complete Hamiltonian (within the d orbitals) for $Cr(NH_3)_6^{3+}$ in a trigonally distorted site is given by eq 1. The first two terms

$$H = H_{FI} + H_{OCT} + H_{VIB} + H_{SO} + H_{D_{3d}} \quad (1)$$

are, respectively, contributions from the free ion and the octahedral ligand field due to the six ammines surrounding the metal. These two terms are solved with spectroscopically determined $10Dq$, B, and C parameters using the matrices of Tanabe and Sugano[7] and give the crystal field terms $|^{2S+1}\Gamma\rangle$. Postponing discussion of the vibrational Hamiltonian H_{VIB} for part C, the next largest term for our system is the spin–orbit interaction H_{SO}. This term splits the 12-fold degeneracy of the $|^4T_{2g}\rangle$ term into four states transforming as Γ_6, Γ_7, Γ_8, Γ_8' (Bethe notation) in the octahedral double group.

The effects of the spin–orbit interaction can be included using degenerate perturbation theory. This is accomplished using an effective Hamiltonian which operates on the 12-fold degenerate components ($|^4T_{2g}\gamma M_S\rangle$, $\gamma = yz, xz, xy$; $M_S = {}^3/_2, {}^1/_2, {}^{-1}/_2, {}^{-3}/_2$) of the $^4T_{2g}$ state. The effective spin–orbit Hamiltonian to second order has the form[8]

$$H_{eff}^{SO} = -\lambda L{\cdot}S + \kappa(L{\cdot}S)^2 + \rho(L_x^2S_x^2 + L_y^2S_y^2 + L_z^2S_z^2) \quad (2)$$

The term in λ gives primarily the first-order splitting, while the terms in κ and ρ come only from second-order contri-

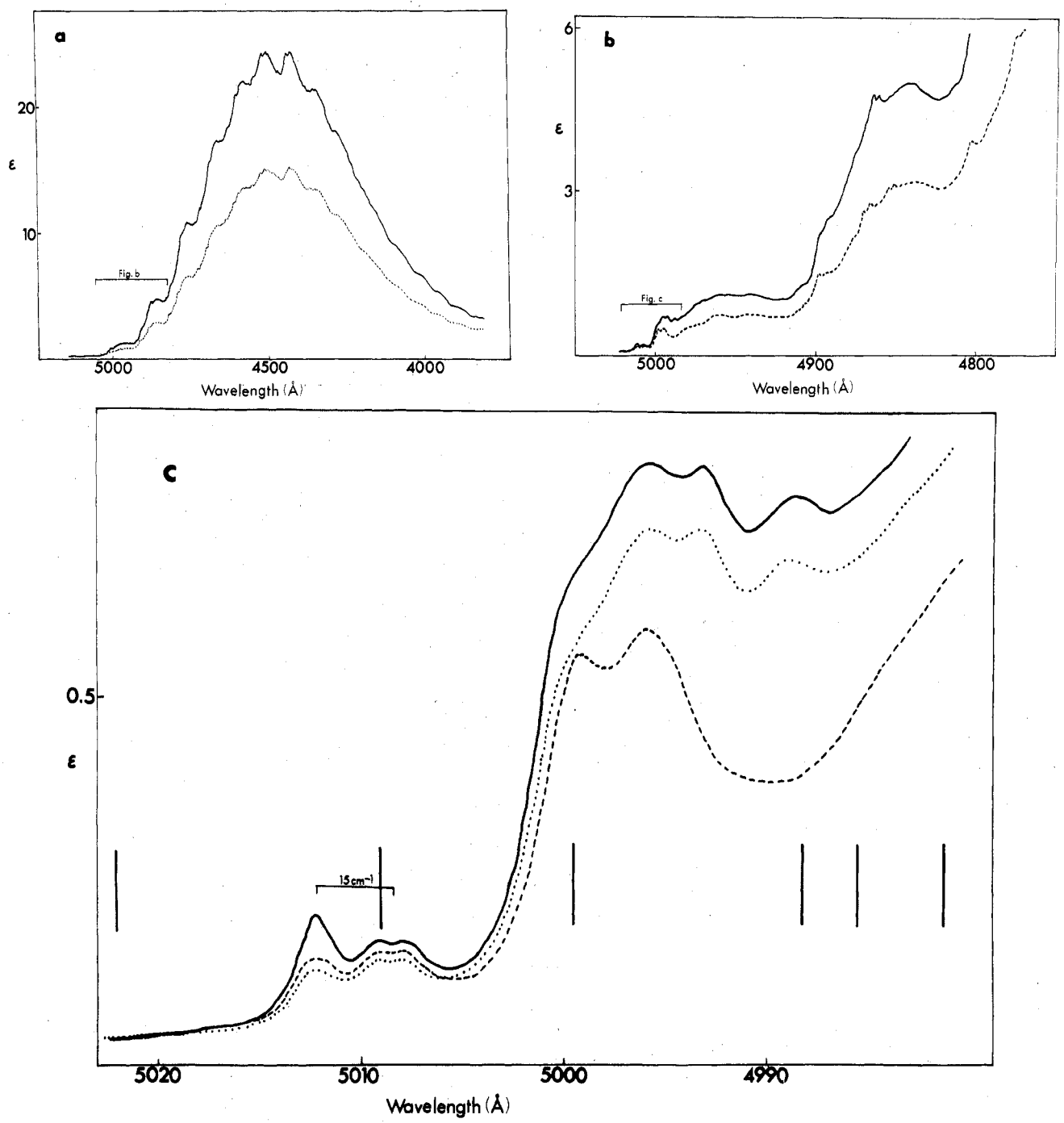

Figure 1. (a) Overall absorption spectrum of the $^4T_{2g} \leftarrow {}^4A_{2g}$ transition in $Cr(NH_3)_6(ClO_4)_2Cl{\cdot}KCl$ at 6 K: solid line, σ polarization; dashed line, π polarization. (b) Low-energy region of the $^4T_{2g} \leftarrow {}^4A_{2g}$ transition, showing the first member of the 403-cm^{-1} progression. Polarizations are as in part a. (c) Blowup of the first 100 cm^{-1} of the $^4T_{2g} \leftarrow {}^4A_{2g}$ transition. The α polarization (dotted line) is for a thinner crystal (×0.9) than those used for the σ and π polarizations. The superimposed vertical lines represent energy levels obtained from solving the effective Hamiltonian of section IV-B.

butions, the ρ term inducing the octahedral symmetry and splitting the Γ_6–Γ_8' pair. The values of λ, κ, and ρ are determined by fitting the energy levels of the effective Hamiltonian to a second-order calculation using the complete d^3 matrices of Runciman and Schroeder.[9] We determine ζ (the reduced one-electron spin–orbit coupling constant necessary for the second-order calculations) from the ground-state g value using the relation[10]

$$g = 2.0023 - \frac{8}{3}\frac{\zeta}{10Dq} \tag{3}$$

Since the second-order calculation is concerned with the zero vibrational levels of the distorted $^4T_{2g}$ excited state and is sensitive to the relative positions of the doublet states, it was necessary to use an excited state $(10Dq)^*$ value in our calculation. (This was estimated by subtracting $2\Delta E$ from the spectroscopic $10Dq$ value, where ΔE is the difference in energy between the magnetic dipole origins and the maximum of the $^4T_{2g}$ absorption band.)

To complete the effective Hamiltonian for the $^4T_{2g}$ state we now add the trigonal distortion term, which is given by the expression

$$H_{\text{eff}}^{D_{3d}} = (-2^{1/2}/2)T(YZ + XZ + XY) \tag{4}$$

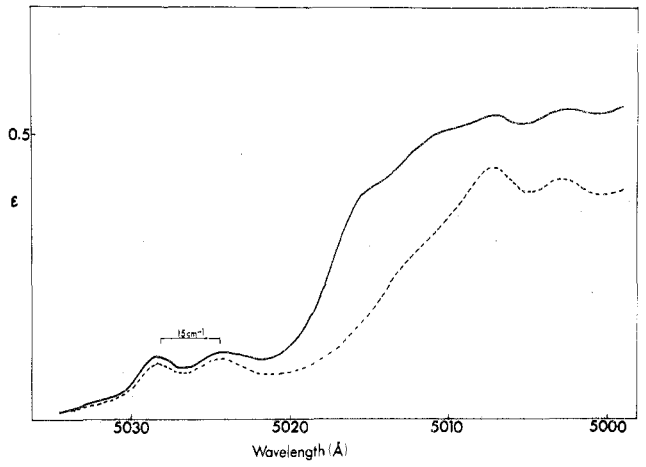

Figure 2. Blowup of the first 100-cm^{-1} region of the $^4T_{2g} \leftarrow {}^4A_{2g}$ transition in $Cr(NH_3)_6(ClO_4)_2Cl{\cdot}RbCl$: solid line, σ polarization; dashed line, π polarization.

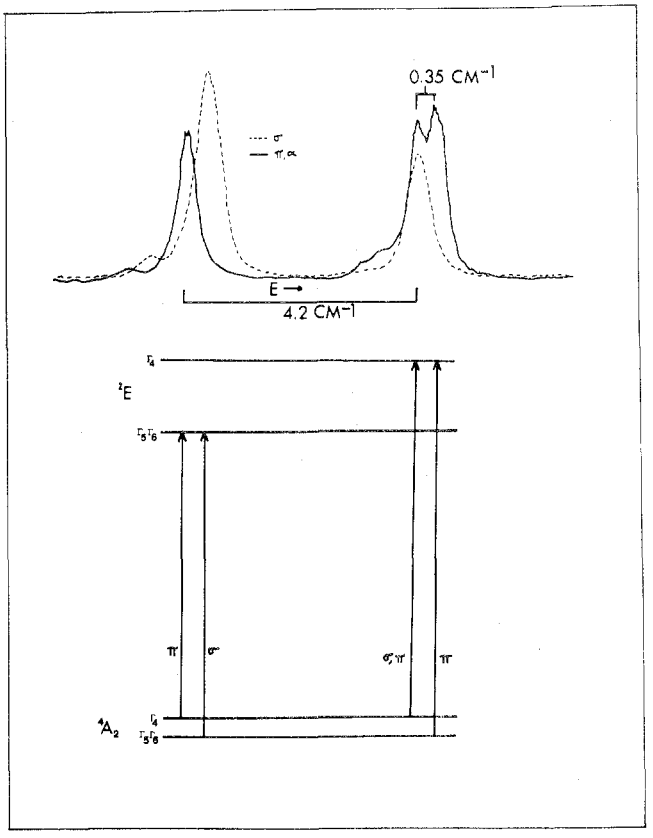

Figure 3. Magnetic dipole (MD) origins of the $^2E_g \leftarrow {}^4A_{2g}$ transition in $Cr(NH_3)_6(ClO_4)_2Cl{\cdot}KCl$ at 6 K. The energy level diagram for this transition is given using the D_{3d} double group. The predicted transition is to be correlated with the MD line directly above.

This term splits the $^4T_{2g}$ (O_h) state into a ^4E_g and a $^4A_{1g}$ (D_{3d}) state, the $^4A_{1g}$ state being lower by $^3/_2T$. The low-symmetry parameter T is determined from the magnetic dipole origins of the $^2E_g(t_{2g}^3)$ state which are split in second order by the combined effects of low-symmetry and spin–orbit coupling (Figure 3). Because of its magnitude, the zero-field splitting (ZFS) of the ground state can be resolved in the transition to the split ^2E_g state. Since a 0.35-cm^{-1} ZFS seemed somewhat large, we felt that further confirmation from low-temperature EPR experiments was appropriate. The ZFS from the EPR spectra of the $^4A_{2g}$ state (of $Cr(NH_3)_6^{3+}$ in $Co(NH_3)_6(ClO_4)_2Cl{\cdot}KCl$ at various doping levels) is temperature dependent and approaches the value observed on the ^2E_g origins at low

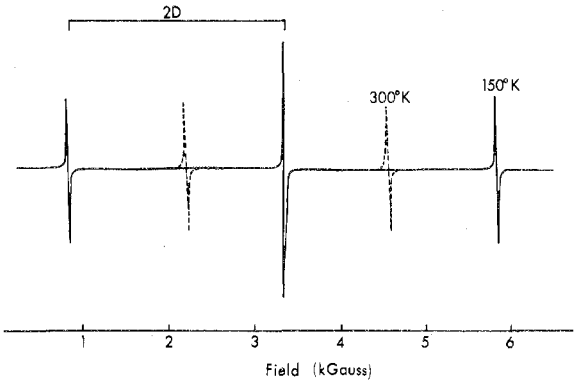

Figure 4. EPR spectrum showing the ($\pm^1/_2 \leftrightarrow \pm^3/_2$) and ($-^1/_2 \leftrightarrow +^1/_2$) transitions of $Cr(NH_3)_6^{3+}$ doped (0.1%) into $Co(NH_3)_6(ClO_4)_2Cl{\cdot}KCl$ at 300 K (dashed lines) and 150 K (solid lines) with $H \parallel c$ axis. The zero-field splitting ($2D$) is ~0.30 cm^{-1} at 150 K and increases with decreasing temperature.

Table I. Effective Hamiltonian Parameters (All in cm^{-1})

$10Dq = 22320$	$\lambda = -30.1$	$\zeta = 195$
$B = 622$	$\kappa = -3.2$	$T(KCl) = +36.7$
$C = 3468$	$\rho = -3.7$	$T(RbCl) = +27.3$

temperature as shown in Figure 4. We then use the magnetic dipole selection rules for the $^2E_g \leftarrow {}^4A_{2g}$ transition to obtain the ordering of the D_{3d} double-group levels shown in Figure 3. Both the sign and magnitude of T are then obtained using the expression[11]

$$\Delta E(\Gamma_4\text{-}\Gamma_5\Gamma_6) = \frac{-4T\zeta}{E(^2E_g) - E(^2T_{2g})} \tag{5}$$

with $E(^2T_{2g})$ given by the previously solved Tanabe–Sugano matrices.

Values of all parameters described in this section are summarized in Table I. Using these parameters, we solve the complete effective Hamiltonian (eq 2 + eq 4) and obtain a splitting pattern for the electronic origins as shown by the vertical lines superimposed in Figure 1c. Obviously, this calculation does not fit the data. We will see in part C that this calculated splitting is strongly affected by the inclusion of H_{VIB} in the effective Hamiltonian, and in particular the large reduction observed requires a sizable Jahn–Teller effect in the $^4T_{2g}$ excited state.

C. Jahn–Teller Effect. Thus far, molecular vibrations of the octahedron have not been included in the effective Hamiltonian for the $^4T_{2g}$ state. It is the interaction of this state with the vibrations which causes the excited state to distort, leading to its broad absorption band shape extending over ~5000 cm^{-1}, rather than the set of lines split by several hundred wavenumbers calculated in the previous section (Franck–Condon effect). Further, inclusion of H_{eff}^{VIB} can also lead to a large reduction of this purely electronic splitting (Ham effect).[12] Since these origins are observable in the absorption spectrum, we have a direct experimental probe of the vibronic distortions of the $^4T_{2g}$ excited state.

The effective Hamiltonian is now extended to include

$$H_{VIB} = \sum_i \frac{P_i^2}{2\mu_i} + \frac{1}{2}k_iQ_i^2 + \left(\frac{\partial V}{\partial Q_i}\right)_0 Q_i \tag{6}$$

The first two terms transform the electronic levels into potential energy surfaces in the coordinates of the octahedral normal modes Q_i with vibrational frequencies $\omega_i = (k_i/\mu_i)^{1/2}$ and require the complete wave functions to be a product of an electronic and a vibrational part (Born–Oppenheimer approximation). The third term in H_{VIB} can be thought of

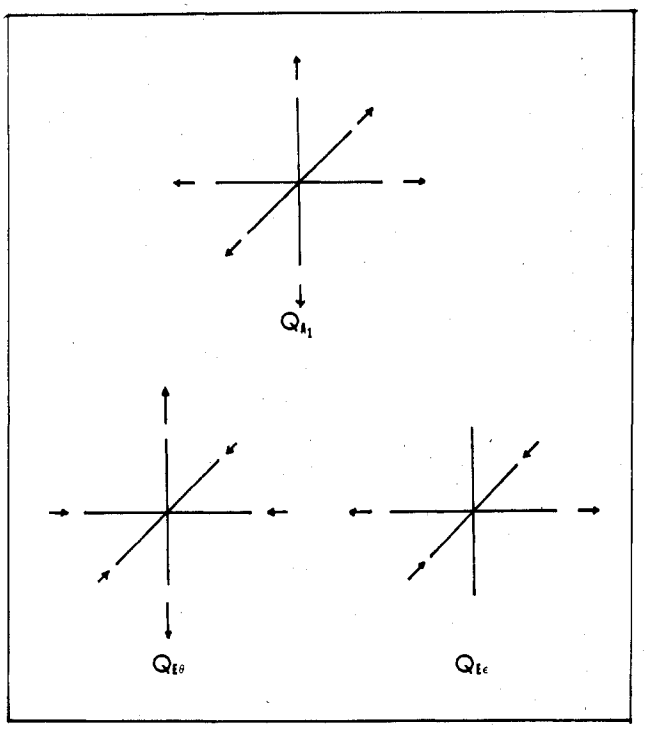

Figure 5. A_{1g} and E_g (θ and ϵ partners) normal modes for an octahedral molecule.

as a force along normal mode Q_i associated with the electronic state Γ

$$F_i = -\langle\Gamma|(\partial V/\partial Q_i)_0|\Gamma\rangle \tag{7}$$

which is balanced by the harmonic restoring forces

$$F_i + k_i\Delta Q_i = 0 \tag{8}$$

at the distorted geometry

$$\Delta Q_i = -F_i/k_i \tag{9}$$

This distortion lowers the energy of the electronic state by an amount

$$E_i = {}^1/_2 k_i(\Delta Q_i)^2 \tag{10}$$

at the equilibrium position. Group theory predicts that for a state of orbital symmetry Γ the term $\langle\Gamma|(\partial V/\partial Q_i)_0|\Gamma\rangle$ can be nonzero only if the mode Q_i transforms as an irreducible representation which is contained in the symmetric direct product $[\Gamma \times \Gamma]$. For the $^4T_{2g}$ state, this means we can only have distortions along the A_{1g}, E_g, and T_{2g} octahedral normal modes. The A_{1g} and θ, ϵ partners of the E_g modes are shown in Figure 5.

Equation 6 is more easily pictured if it is rewritten[13,14] specifically considering each of the orbital partners (yz, xz, xy) of the $^4T_{2g}$ state as basis functions. By use of the Wigner–Eckart theorem, the effective Hamiltonian becomes

$$H_{\text{eff}}^{\text{VIB}} = \sum_i \frac{P_i^2}{2\mu_i} + \frac{1}{2}k_iQ_i^2 +$$

$$\langle {}^4T_{2g}\|\frac{\partial V}{\partial Q_{A_{1g}}}\|{}^4T_{2g}\rangle \begin{pmatrix} Q_{A_{1g}} & 0 & 0 \\ 0 & Q_{A_{1g}} & 0 \\ 0 & 0 & Q_{A_{1g}} \end{pmatrix} +$$

$$\langle {}^4T_{2g}\|\frac{\partial V}{\partial Q_{E_g}}\|{}^4T_{2g}\rangle \times$$

$$\begin{pmatrix} \frac{1}{2}Q_{E_g\theta} - \frac{3^{1/2}}{2}Q_{E_g\epsilon} & 0 & 0 \\ 0 & \frac{1}{2}Q_{E_g\theta} + \frac{3^{1/2}}{2}Q_{E_g\epsilon} & 0 \\ 0 & 0 & -Q_{E_g\theta} \end{pmatrix} +$$

$$\langle {}^4T_{2g}\|\frac{\partial V}{\partial Q_{T_{2g}}}\|{}^4T_{2g}\rangle \begin{pmatrix} 0 & Q_{T_{2g}\zeta} & Q_{T_{2g}\eta} \\ Q_{T_{2g}\zeta} & 0 & Q_{T_{2g}\xi} \\ Q_{T_{2g}\eta} & Q_{T_{2g}\xi} & 0 \end{pmatrix} \tag{11}$$

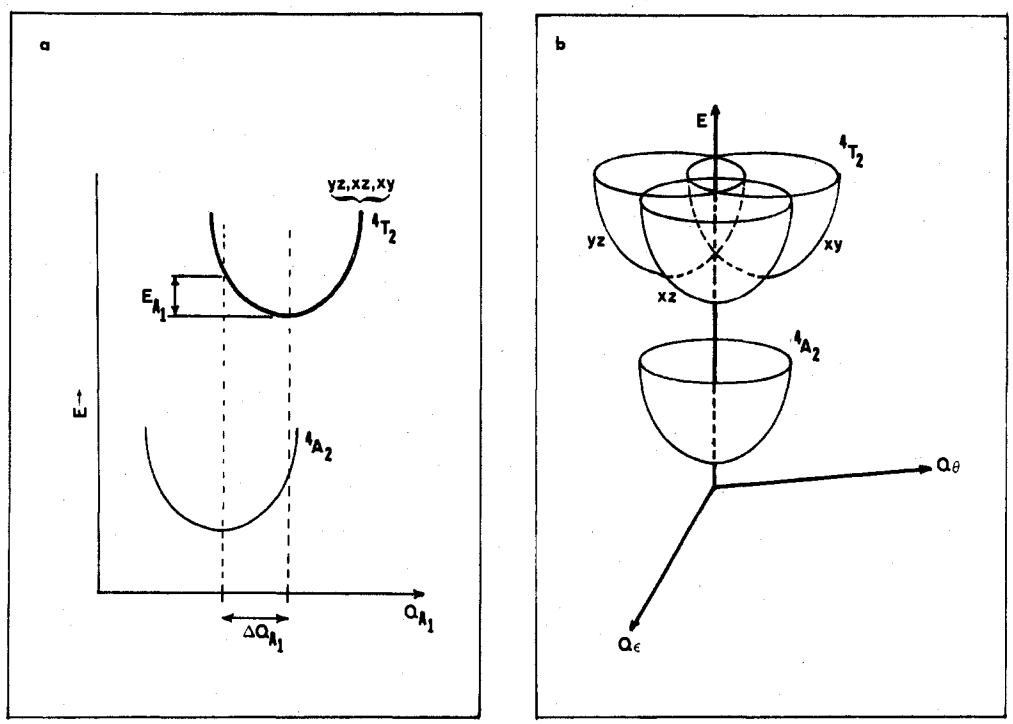

Figure 6. (a) Potential energy surfaces along the A_{1g} mode for the $^4T_{2g}$ state displaced by ΔQ_{A_1} from the ground-state geometry. (b) Potential energy surfaces along the E_g mode (θ and ϵ partners) for the $^4T_{2g}$ excited state undergoing an E_g Jahn–Teller distortion relative to the octahedral ground state.

Coupling to the A_{1g} mode is seen from eq 11 to be diagonal, displacing all three electronic partners equally in $Q_{A_{1g}}$ space. This leads to the distortion shown in Figure 6a but produces no electronic mixing. Such a distortion has no effect on the energies of the $^4T_{2g}$ electronic Hamiltonian but shifts the excited-state geometry relative to the ground state and thus contributes to the vibrational progression.

The E_g force is also seen to be diagonal in the electronic partners, but each partner is distorted along a different direction in $Q_{E_g\theta}$, $Q_{E_g\epsilon}$ space and therefore electronically pure, but spacially separated (Figure 6b). As with the A_{1g} mode this distortion contributes to the Franck–Condon progression. In addition, it has the important effect of reducing the effective Hamiltonian matrix elements between different partners by the overlap of the zeroth vibrational levels of the displaced harmonic oscillator wave functions. This Ham[12] reduction factor is

$$R_{E_g} = e^{-(3/2)S_{E_g}} \tag{12}$$

where $S_{E_g} = E_{E_g}/\hbar\omega_{E_g}$, quenching the values of the terms in λ and T and the off-diagonal part of κ. Matrix elements diagonal within a (yz, xz, xy) basis are not affected (ρ and the diagonal part of κ).

The T_{2g} vibronic matrix cannot be diagonalized within the (yx, xz, xy) basis functions of the $^4T_{2g}$ state but leads to four equivalent trigonal distortions. In particular, the T_{2g} Jahn–Teller effect only slightly reduces the trigonal ligand field by an approximate factor[15] of

$$R^{Trig}_{T_{2g}} = {}^2/_3 + {}^1/_3 e^{-(9/4)E_{T_{2g}}/\hbar\omega_{T_{2g}}} \tag{13}$$

Nontrigonal matrix elements of the effective Hamiltonian are strongly quenched by the factor

$$R_{T_{2g}} = e^{-(9/4)E_{T_{2g}}/\hbar\omega_{T_{2g}}} \tag{14}$$

We can now use the data in part A to eliminate the possibility of a significant T_{2g} Jahn–Teller distortion. From parallel studies of the ^2E_g and $^4A_{2g}$ zero-field splittings of the KCl and RbCl salts, we find a change in the magnitude of the trigonal distortion (ΔT) between the two salts of 10 cm^{-1}. If a T_{2g} Jahn–Teller effect were responsible for the reduction in the splittings of the magnetic dipole lines, we would expect the trigonal term in the effective Hamiltonian to be reduced to no less than two-thirds of its original value. The minimal expected change of 7 cm^{-1} ($\Delta T \cdot R^{Trig}_{T_{2g}}$) between salts would produce a measurable change in the splittings of the magnetic dipole origins. Comparison between Figures 1c and 2 shows that no change in these splittings is observed.

Using eq 12, 2, and 4 (and the higher order $G(x)$ and $G(x/2)$ terms given by Ham[12]) we now calculate the E_g Jahn–Teller distortion required to reduce the spin–orbit and low-symmetry parameters of the effective Hamiltonian in order to fit the magnetic dipole splittings observed in Figure 1c. The effect of varying the magnitude of the Jahn–Teller distortion is shown in Figure 7. The left-hand side of this diagram corresponds to no Jahn–Teller distortion and the energy spacings correspond to the vertical lines in Figure 1c. We see from Figure 7 that as S_{E_g} becomes large, the levels asymptotically converge into two groups, with the limiting splitting determined by $-2(\rho + \kappa)$, the second-order terms. This prediction agrees well with the observed absorption spectrum, Figure 1c, and we find a good fit of the data is obtained with $S_{E_g} = 2.3 \pm 0.3$.

D. Franck–Condon Analysis. Having obtained a value of S_{E_g} from the quenching of the magnetic dipole lines, we are now in a position to determine the contribution from the E_g distortion to the overall band shape of the $^4T_{2g} \leftarrow {}^4A_{2g}$ transition. Any differences between the observed and calculated band shapes can only be due to additional contributions from the A_{1g} distortion allowing this to be experimentally obtained.

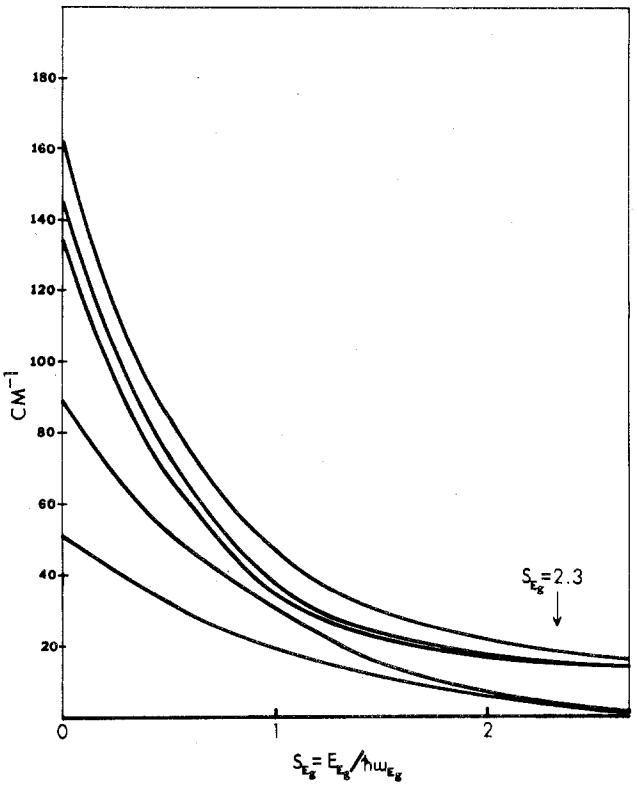

Figure 7. Effects of increasing the E_g Jahn–Teller distortion (given by the parameter S) on the spin–orbit plus low-symmetry-split $^4T_{2g}$ origins.

Several factors must be considered in generating an accurate band shape.[6] First, each magnetic dipole line will act as an origin for progressions in each of the distorting modes. The form of the progression in one distorting mode is given by the Poisson distribution

$$I_n = \frac{S^n}{n!} e^{-S} \tag{15}$$

with I_n being the intensity of the nth quantum. In addition, the polarized spectra in Figure 1 show that the overall band is electric dipole allowed, requiring most of the intensity to come from coupling to odd-parity vibrations. For the CrN_6 skeleton there are 3 odd-parity modes (2 T_{1u} and 1 T_{2u}) which can induce vibronic intensity. Addition of the 18 ammine hydrogens provides 10 additional odd-parity modes. In principle, one vibrational quantum in each of these modes can couple to each magnetic dipole origin. Each would serve as origins for Franck–Condon progressions as given by eq 15 in each distorting mode. The relative importance of these odd-parity modes in inducing intensity must be determined from experiment. The transition to the $^4T_{2g}$ state, although highly structured, still does not allow resolution of all the vibronic origins, owing to their overlap and broadness (Figure 1b). This can be overcome, however, by the use of the $^2E_g(t_{2g}^3)$ state as a probe of the vibronic origins of the $^4T_{2g}$ state. The ^2E_g state is coupled in second order by the spin–orbit operator to the $^4T_{2g}$ state. Flint's studies[16] strongly support the idea that almost all of the vibronic intensity of the ^2E_g originates from this coupling. Thus, the vibronic bands of the $^2E_g \leftarrow {}^4A_{2g}$ transition were used (as indicated in Figure 8) for the $^4T_{2g}$ state.

One final point should be made. The A_{1g} and E_g vibrations have similar energies in the ground state (462 and 412 cm^{-1},

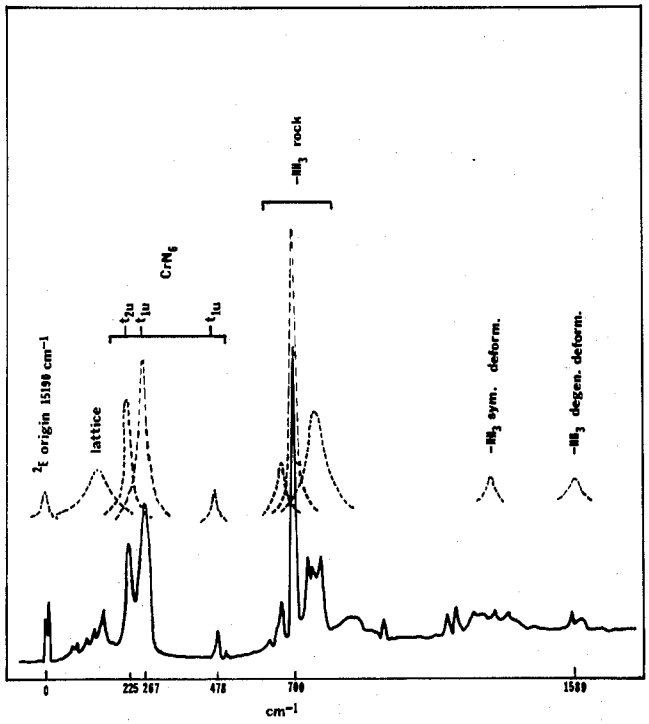

Figure 8. Absorption spectrum of the overall $^2E_g \leftarrow {}^4A_{2g}$ transition of $Cr(NH_3)_6(ClO_4)_2Cl{\cdot}KCl$ at 6 K (solid line). The dotted lines represent the origins used in generating the band shape of the $^4T_{2g} \leftarrow {}^4A_{2g}$ transition (Figure 9). Contributions from $^2T_{1g}$ have been eliminated from the band shape origins by comparison to the emission and the RbCl absorption spectra. General vibrational regions are indicated above.

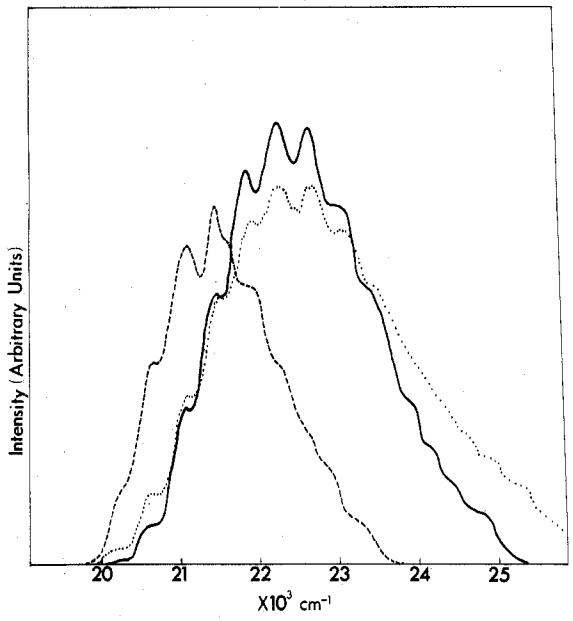

Figure 9. Comparison of the experimental band shape (dotted line) with the generated band shape for $S = 2.3$ (dashed line) and $S = 5.0$ (solid line). The dashed curve was scaled down by a factor of $^3/_5$.

respectively[17]) which should be decreased somewhat in the $^4T_{2g}$ excited state. In Figure 1a we see that the $^4T_{2g} \leftarrow {}^4A_{2g}$ transition exhibits one main progression in a 403-cm^{-1} vibration. We can then use the Huang–Rhys approximation[18] that these two vibrations are degenerate with an energy equal to the characteristic 403-cm^{-1} vibration observed in the absorption spectrum. The overall band shape is then obtained as previously described using eq 15 with $S = S_{A_{1g}} + S_{E_g}$. Figure 9 demonstrates that the E_g contribution alone ($S = 2.3$) cannot account for all of the excited-state distortion. A best fit to experiment gives $S = 5.0 \pm 0.4$. Thus, a large contribution from the A_{1g} distortion ($S_{A_{1g}} = 2.7 \pm 0.5$) is also obtained.

E. Excited-State Geometry. Using our experimentally determined $S_{A_{1g}}$ and S_{E_g} and eq 10, we obtain reasonable estimates for the magnitudes of the excited-state distortions in these modes: $|\Delta Q_E| = 0.15 \pm 0.01$ Å, $|\Delta Q_{A_{1g}}| = 0.16 \pm 0.02$ Å. These are experimentally obtained parameters which have not relied on any particular model and have required only a few reasonable approximations. The error estimates of $\Delta Q_{A_{1g}}$ and ΔQ_{E_g} ($\simeq 10\%$) are, however, still subject to the approximations used in our theoretical treatment. The accuracy of the effective Hamiltonian approach is limited most by our ability to estimate the necessary parameters for the electronic origins of the relaxed $^4T_{2g}$ excited state. Our use of an excited state $(10Dq)^*$, while certainly a simplification, seems the most reasonable way to obtain these parameters, with small errors not being very important in our estimate of S. Finally, the inclusion of vibronic effects has required a crude adiabatic approximation with harmonic forces, linear electronic–nuclear coupling, etc. The sign of $|\Delta Q_i|$ is now easily obtained from group theory and the $^4T_{2g}$ wave functions.[14]

We first consider the A_{1g} distortion. From eq 11 and Figure 6a, the three partners of the $^4T_{2g}$ state are distorted in the same way in the A_{1g} space. We then need consider only one partner, e.g., xy. Here we are interested in the force $\partial V/\partial Q_{A_{1g}}$ in the excited state relative to that in the ground state

$$F_{A_{1g}}{}^{T_{2g}} - F_{A_{1g}}{}^{A_{2g}} = -\langle {}^4T_{2g}xy|\frac{\partial V}{\partial Q_{A_{1g}}}|{}^4T_{2g}xy\rangle + \langle {}^4A_{2g}|\frac{\partial V}{\partial Q_{A_{1g}}}|{}^4A_{2g}\rangle \quad (16)$$

which can be rewritten in terms of one-electron wave functions

$$F_{A_{1g}}{}^{T_{2g}} - F_{A_{1g}}{}^{A_{2g}} = -\langle\epsilon|\frac{\partial V}{\partial Q_{A_{1g}}}|\epsilon\rangle + \langle\zeta|\frac{\partial V}{\partial Q_{A_{1g}}}|\zeta\rangle \quad (17)$$

since

$$|{}^4A_{2g}\rangle = -|\xi\eta\zeta|$$

$$|{}^4T_{2g}xy\rangle = -|\xi\eta\epsilon|$$

and ξ, η, ζ, θ, and ϵ are the one-electron yz, xz, xy, z^2, and $x^2 - y^2$ orbitals, respectively. This involves excitation of a t_{2g} electron into an antibonding e_g orbital and therefore requires the ligands to expand. It is interesting to use a ligand field calculation to predict the observed splitting. Evaluating

$$\frac{\partial V}{\partial Q_{A_{1g}}} = \frac{175e^2}{4(6^{1/2}R^6)}(x^4 + y^4 + z^4 - \frac{3}{5}r^4) \quad (18)$$

over the previous wave functions gives[14]

$$F_{A_{1g}} = -\frac{50Dq}{6^{1/2}R} \quad (19)$$

Experimental values for Dq and R then give $\Delta Q_{A_{1g}} = 0.27$ Å which is larger by a factor of about 2 than the experimental value of 0.16 Å. Similar comparisons between theory and experiment have been previously noted.[14]

The picture becomes more complicated for the E_g mode as each $^4T_{2g}$ partner distorts along a different direction in $Q_{E_g\theta}, Q_{E_g\epsilon}$ space (eq 11, Figure 6b). These distortions, however, are related by symmetry and are simply $E_g\theta$ type distortions, Figure 5, with the unique axis pointed along each of the three

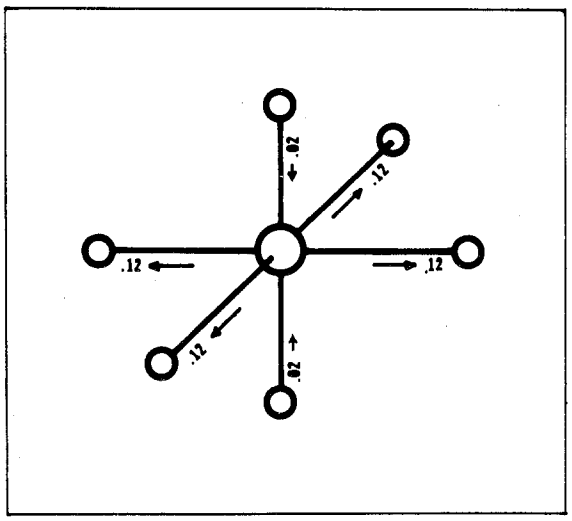

Figure 10. Equilibrium geometry for $Cr(NH_3)_6^{3+}$ in the $^4T_{2g}$ excited state. The numbers indicate the bond length changes in angstroms from the ground-state values of 2.06 Å in the directions indicated by the arrows.

axes of the octahedron. Continuing to consider the xy partner gives

$$F_{E_g\theta}{}^{T_{2g}} - F_{E_g\theta}{}^{A_{2g}} = -\langle\epsilon|\frac{\partial V}{\partial Q_{E_g\theta}}|\epsilon\rangle + \langle\zeta|\frac{\partial V}{\partial Q_{E_g\theta}}|\zeta\rangle \qquad (20)$$

A similar qualitative picture of an electron going from an xy into an $x^2 - y^2$ orbital gives the $E_g\theta$ distortion with the x and y ligands going out and the z ligands going inward (i.e., the sign of $Q_{E_g\theta}$ is negative).

We combine these normal-mode distortions into changes of the octahedral axes x, y, and z using the transformation

$$\begin{pmatrix}\Delta x\\ \Delta y\\ \Delta z\end{pmatrix} = \frac{1}{2}\begin{pmatrix}\left(\frac{2}{3}\right)^{1/2} & -\frac{1}{3^{1/2}} & -1\\ \left(\frac{2}{3}\right)^{1/2} & -\frac{1}{3^{1/2}} & 1\\ \left(\frac{2}{3}\right)^{1/2} & \frac{2}{3^{1/2}} & 0\end{pmatrix}\begin{pmatrix}\Delta Q_{A_{1g}}\\ \Delta Q_{E_g\theta}\\ \Delta Q_{E_g\epsilon}\end{pmatrix} \qquad (21)$$

where Δx, Δy, and Δz are the bond length charges in the x, y, and z directions, respectively. This gives the $^4T_{2g}$ excited-state equilibrium geometry pictured in Figure 10.

V. Discussion

In the previous section we have experimentally determined that the $^4T_{2g}$ state undergoes a rather large distortion along both A_{1g} and E_g normal modes leading to the D_{4h} complex in Figure 10. The detailed spectroscopy required a low-temperature single-crystal sample form. A statement concerning the relevance of these results to $Cr(NH_3)_6^{3+}$ in aqueous solution is now in order.

The $^4T_{2g} \leftarrow {}^4A_{2g}$ ligand field transition involves changes in electronic structure predominantly localized on the central metal. Since only these and group theory determine the direction and magnitude of distorting forces, these should not be very sensitive to outer coordination effects. The magnitude of the distortion is controlled (equation 8) by the balance of these forces and the harmonic oscillator restoring forces along the normal modes. Thus, the magnitude of these distortions might be expected to increase upon going from the low-temperature crystal to a solution environment. Vibrational studies[17] indicate that these changes in force constant are between 5% and 10% in the ground state.

Our spectroscopic studies have been concerned with hexaamminechromium(III). The extension of these results to the excited-state distortions of ligand-substituted molecules is straightforward. Ligand substitution along the z axis of the octahedron splits the $^4T_{2g}$ state into $^4B_{2g}$ and ^4E_g, the ^4E_g state lying lower in energy (for $Dq_{ax} < Dq_{eq}$) as determined by polarized spectral studies.[19] A transition to this state excites the yz and xz partners of the $^4T_{2g}$ parent state. The diagonal nature of eq 11 means that the distorting forces will not be affected strongly by the D_{4h} or C_{4v} nature of the ligand-substituted complex. The distortions associated with the yz and xz partners (eq 11) will have the same form as shown in Figure 10 but with the undistorted axis now directed along the x and y axes, respectively, of the D_{4h} (C_{4v}) complex. This will lead to significant elongation of both the axis containing the substituted ligand and one perpendicular axis. Further localization of the distortion along one reaction coordinate remains the subject of future studies; however, one can see that this distortion (Figure 10) will produce a large Franck–Condon factor in the direction of the observed ligand photodissociation product. These studies are now being extended to other ligand field spectroscopic problems of photochemical importance.

Acknowledgment. We are grateful to the Research Corp. for providing the funding necessary for our optical spectroscopy system. This work has also been supported by the Cabot Solar Energy Fund and by an Alfred P. Sloan Research Fellowship (E.I.S.). We thank Professors Mark Wrighton and Bob Silbey for useful discussions and Steve Rice for the EPR studies.

Registry No. $Cr(NH_3)_6(ClO_4)_2Cl{\cdot}KCl$, 66269-58-7; $Cr(NH_3)_6(ClO_4)_2Cl{\cdot}RbCl$, 66269-57-6.

References and Notes

(1) E. Zinato in "Concepts of Inorganic Photochemistry", A. W. Adamson and P. D. Fleischauer, Ed., Wiley-Interscience, New York, N.Y., 1975, Chapter 4, p 143.
(2) A. W. Adamson, *J. Phys. Chem.*, **71**, 798 (1967).
(3) M. S. Wrighton, H. B. Gray, and G. S. Hammond, *Mol. Photochem.*, **5**, 165 (1973).
(4) J. I. Zink, *J. Am. Chem. Soc.*, **94**, 8039 (1972).
(5) B. Foxman, R. B. Wilson, and E. I. Solomon, to be submitted for publication.
(6) E. I. Solomon and C. J. Ballhausen, *Mol. Phys.*, **29**, 279 (1975).
(7) Y. Tanabe and S. Sugano, *J. Phys. Soc. Jpn.*, **9**, 753 (1954).
(8) M. D. Sturge, *Phys. Rev. B*, **1**, 1005 (1970).
(9) W. A. Runciman and K. A. Schroeder, *Proc. R. Soc. London, Ser. A*, **265**, 489 (1962).
(10) S. Sugano, Y. Tanabe, and H. Kamimura, "Multiplets of Transition-Metal Ions in Crystals", Academic Press, New York, N.Y., 1970, p 202.
(11) S. Sugano and Y. Tanabe, *J. Phys. Soc. Jpn.*, **13**, 880 (1958).
(12) F. S. Ham, *Phys. Rev.* [*Sect.*] *A*, **138**, 1727 (1965).
(13) M. D. Sturge, *Solid State Phys.*, **20**, 91 (1967).
(14) E. I. Solomon and D. S. McClure, *Phys. Rev. B*, **9**, 4690 (1974).
(15) M. Caner and R. Englman, *J. Chem. Phys.*, **44**, 4054 (1966).
(16) C. D. Flint and P. Greenough, *J. Chem. Soc., Faraday Trans. 2*, **68**, 897 (1972).
(17) (a) H. Siebert and H. Eysel, *J. Mol. Struct.*, **4**, 29 (1969); (b) K. H. Schmidt and A. Müller, *Inorg. Chem.*, **14**, 2183 (1975); (c) K. Nakamoto, "Infrared Spectra of Inorganic and Coordination Compounds", 2nd ed, Wiley, New York, N.Y., 1971, p 150.
(18) D. B. Fitchen in "Physics of Color Centers", W. B. Fowler, Ed., Academic Press, New York, N.Y., 1968, p 293.
(19) (a) L. Dubicki and P. Day, *Inorg. Chem.*, **10**, 2043 (1971); (b) R. L. Klein, N. C. Miller, and J. R. Perumareddi, *Inorg. Chim. Acta*, **7**, 685 (1973).